Original Article

Comparison and combination of amide proton transfer magnetic resonance imaging and the apparent diffusion coefficient in differentiating the grades of prostate cancer

Xiaoyan Qin[1#], Ronghua Mu[1#], Wei Zheng[1,2#], Xin Li[1], Fuzhen Liu[1], Zeyu Zhuang[1,2], Peng Yang[1], Xiqi Zhu[1]

[1]Department of Radiology, Nanxishan Hospital of Guangxi Zhuang Autonomous Region, Guilin, China; [2]Department of Radiology, Graduate School of Guilin Medical University, Guilin, China

Contributions: (I) Conception and design: X Qin, X Zhu, R Mu, W Zheng; (II) Administrative support: X Zhu, X Qin; (III) Provision of study materials or patients: X Qin, X Zhu, R Mu, W Zheng, X Li; (IV) Collection and assembly of data: X Qin, F Liu, Z Zhuang, P Yang; (V) Data analysis and interpretation: X Qin, R Mu, W Zheng; (VI) Manuscript writing: All authors; (VII) Final approval of manuscript: All authors.

[#]These authors contributed equally to this work.

Correspondence to: Xiqi Zhu, MD, PhD. Department of Radiology, Nanxishan Hospital of Guangxi Zhuang Autonomous Region, No. 46, Chongxin Road, Guilin 541004, China. Email: xiqi.zhu@163.com.

Background: More effective risk stratification of prostate cancer (PCa) than that possible with current methods can reduce undertreatment and guard against overtreatment. The aim of this study is to validate the differences and combined effects of amide proton transfer (APT) imaging and apparent diffusion coefficient (ADC) in discriminating the PCa grade group (GG) ≤2 from GG ≥3 PCa.

Methods: This is an ongoing prospective study conducted in the radiology department of Nanxishan Hospital of Guangxi Zhuang Autonomous Region. Patients pathologically diagnosed with PCa were enrolled consecutively according to the eligibility criteria. A total of 180 patients (age range, 42–92 years) were included in this study. Using histopathology as the reference standard, we placed 71 cases in GG ≤2 (mean age 67.03±8.696 years) and 109 cases in GG ≥3 (age 69.60±9.638 years). Magnetic resonance imaging (MRI) parameters, including APT and ADC values, were analyzed using an independent samples *t*-test and binary logistic regression analysis stratified with GG. Receiver operating characteristic curve was used to analyze the diagnostic performance for different parameters distinguishing GG ≤2 and GG ≥3.

Results: APT [odds ratio (OR) for the transitional zone (TZ) PCa: 3.20, 95% CI: 1.14–8.98, P=0.02; OR for the peripheral zone (PZ) PCa: 86.32, 95% CI: 13.24–562.88, P=0.003] and ADC values (OR for TZ PCa: 89.79; 95% CI: 2.85–2,827.99, P=0.01; OR for PZ PCa: 39.92; 95% CI: 3.22–494.18, P=0.004) were independent predictors that differentiated the GG of patients. The sensitivity and specificity of the APT values were 61.1% and 81.0%, respectively, while the sensitivity and specificity of the ADC values were 83.3% and 61.9%, respectively. The optimal cutoff value of APT was 3.35% and which of ADC was 1.25×10^{-3} mm^2/s in TZ origin PCa. At the optimal cutoff values of 3.31% (APT) and 0.79×10^{-3} mm^2/s (ADC) in PZ PCa, the sensitivity and specificity of the APT values were 74.0% and 83.6%, respectively, while the sensitivity and specificity of the ADC values were 94.0% and 53.4%, respectively. The area under the curve of the combination of APT and ADC was significantly higher than either of APT or ADC alone in Delong test (TZ: P=0.002 and P=0.020; PZ: P=0.033 and P<0.001).

Conclusions: APT and ADC have complementary effects on the sensitivity and specificity for identifying different PCa GGs. A combination model of APT and ADC could improve the diagnostic efficacy of PCa differentiation.

Keywords: Amide proton transfer (APT); apparent diffusion coefficient (ADC); prostate cancer (PCa); grade group

Submitted Jul 07, 2022. Accepted for publication Nov 29, 2022. Published online Dec 08, 2022.
doi: 10.21037/qims-22-721
View this article at: https://dx.doi.org/10.21037/qims-22-721

Introduction

Since the introduction of cancer screening using the prostate-specific antigen (PSA) test and early diagnosis by targeted biopsy, prostate cancer (PCa)-specific mortality has decreased, but overdiagnosis and overtreatment of this tumor have increased (1). Better risk stratification of PCa is needed to improve the detection of clinically significant PCa (2). Active surveillance has rapidly evolved to become the standard of care for low-risk PCa and a cautious option for favorable-risk PCa (3,4). However, there is growing concern about how far the boundaries of case selection can be pushed safely and how to define the role of imaging markers in the routine care of patients with PCa (5).

Prostate multiparametric magnetic resonance imaging (MRI) is a useful risk stratification tool that is strongly recommended for baseline assessment of PCa. MRI is often used in the diagnosis and staging of PCa (3,6,7). In particular, the apparent diffusion coefficient (ADC), which is derived from diffusion-weighted imaging (DWI) and which corresponds to the cellular density within tumors, has shown a significant correlation with the grade group (GG) of PCa (8). However, there is wide variability in ADC values depending on the prostatic zone and considerable interpatient variability within the same zone (9). A wide range of ADC cutoff values have been reported, and there is substantial overlap corresponding to different GGs of risk (9). Theoretically, newly available MRI tools will allow for clinicians to tailor best management strategy for men with PCa (6,10). Amide proton transfer (APT) has been introduced as a novel endogenous contrast mechanism for MRI, in which the proteins and peptides in tissues or tumors that contain abundant amide chemical constituents are detected. APT values have been reported to have the potential to be diagnostic biomarkers and stage predictors of PCa and other tumors (11,12).

A previous study reported that the APT signal could complement the ADC for grading glioma (13). Consequently, we speculated that APT and ADC have different sensibilities and specificities to distinguish the degree of differentiation of PCa. We further hypothesized that a combined model of APT and ADC could better identify those PCa patients at low or favorable risk. The purpose of this study is to identify whether there are differences in the diagnostic efficacy between APT and ADC values in discriminating GG ≤2 from GG ≥3 PCa and to further study whether the combined model of the 2 parameters can improve the diagnostic efficacy. We further aim to determine whether APT and ADC have different diagnostic efficacy in PCa originating in different zones to verify the stability and repeatability of the diagnostic efficacy of APT and ADC. We present the following article in accordance with the STARD reporting checklist (available at https://qims.amegroups.com/article/view/10.21037/qims-22-721/rc).

Methods

Patients

This study is part of an ongoing prospective investigation of PCa using multiparametric MR and has been conducted in accordance with the Declaration of Helsinki (as revised in 2013). The study was approved by the local Ethics Committee of Nanxishan Hospital of Guangxi Zhuang Autonomous Region, and all participants signed an informed consent form.

From January 2020 to April 2022, patients pathologically diagnosed with PCa in Nanxishan Hospital of Guangxi Zhuang Autonomous Region were selected consecutively. All enrolled patients underwent multiparametric MRI of the prostate. Pathological results originated from pathological examination of prostate prostatic tissue obtained by prostate biopsy and/or radical prostatectomy. Patients were included if they had not undergone hormone or radiation treatment, had no MRI contraindication, and underwent biopsy and/or radical prostatectomy no more than 1 month after undergoing multiparametric MR imaging. Patients were excluded if they had other serious organ diseases or mental illnesses and/or the quality of their MRI was poor. A flowchart of the patient enrolment process is shown in *Figure 1*.

Multiparametric MRI

All scans were performed using a 3.0T (Ingenia

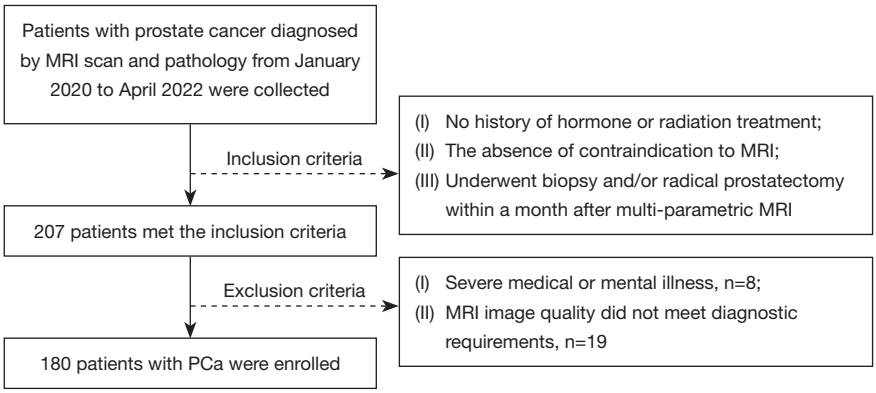

Figure 1 Flowchart of study participant selection. MRI, magnetic resonance imaging; PCa, prostate cancer.

Table 1 Scan sequences of multiparametric MRI

Scan protocol	Scan sequences	TR (ms)	TE (ms)	FOV (mm^2)	Slice thickness (mm)	Number of slices	Matrix	Scan time (min)
T1	TSE	450	10	200×200	3	24	308×264	1.34
T2	TSE	2,218	100	200×200	3	28	364×304	2.20
APT	TSE	5,000	8.3	100×100	8	10	64×45	7.00
DWI	EPI	3,826	69	200×200	3	28	152×125	4.47
T2*	mFFE	6	1.1	350×100	3	80	152×125	0.25

APT, amide proton transfer; DWI, diffusion weighted imaging; EPI, echo planar imaging; FOV, field of view; mFFE, multiple fast field echo; MRI, magnetic resonance imaging; T2*, quantitative T2*; TE, echo time; TR, repetition time; TSE, turbo spin echo.

3.0 CX; Philips Healthcare, Best, the Netherlands) with a 16-channel phased-array body coil. Scan sequences are shown in *Table 1*. During the DWI sequence scanning, *b* values used for DWI always included 0, 100, 400, and 800, and 1,400 mm/s^2 with the automatic calculation of the ADC map.

Spatial saturation pulses, known as the regional saturation technique (REST), were applied to suppress the MR signal from moving tissues outside the imaged volume to reduce or eliminate motion artifacts. Four REST slabs were used during APT scanning. Two of them were placed on the bladder and rectum to reduce the motion artifacts. The other 2 were placed on the left and right iliac crest to improve the uniformity of the B1 field. Their angulation, center, and width were adjusted according to the size of the patient (*Figure 2*).

Image analysis

Each examination was retrospectively reviewed on the postprocessing workstation of the IntelliSpace Portal version 8 (Philips Healthcare). All pulse sequences were available at the time of the imaging review. Two experienced radiologists (X Zhu and X Qin, with 21 and 15 years of abdominal radiology experience, respectively) who were blinded to the final histopathology results and clinical information reviewed all of the MR images and discusses them until a consensus was reached. Region of interest (ROI) was delineated in the maximum level of the lesion and its 2 consecutive layers. The ROI outlined the most foci possible. The mean values of each lesion's ROI in 3 consecutive layers were recorded as variable values of APT, ADC, and T2* time (*Figure 3*). Manual adjustments were made as needed to ensure the choice of ROI in different protocol images was at the same foci level. Copy and paste functions were used to ensure the consistency of the size, shape, and position of the ROIs. The ADC maps were calculated based on DWIs with different *b* values. For patients with multiple PCa lesions, the largest PCa lesion was selected for analysis (14). First, 2 radiologists identified

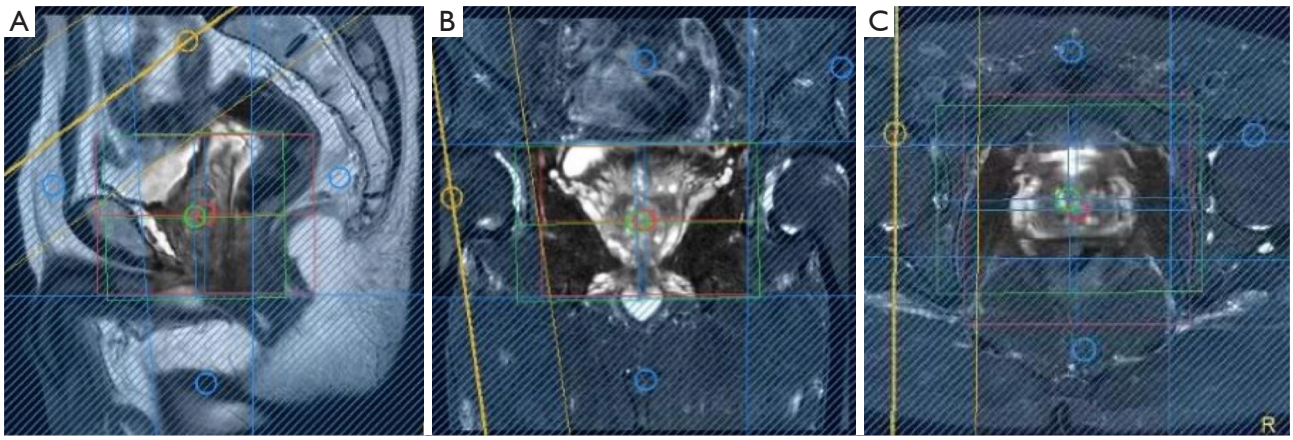

Figure 2 Indication of REST slabs that were used during the amide proton transfer sequence scanning. (A) REST slabs in the sagittal section. (B) REST slabs in the coronal section. (C) REST slabs in the transversal section. REST, regional saturation technique; APT, amide proton transfer.

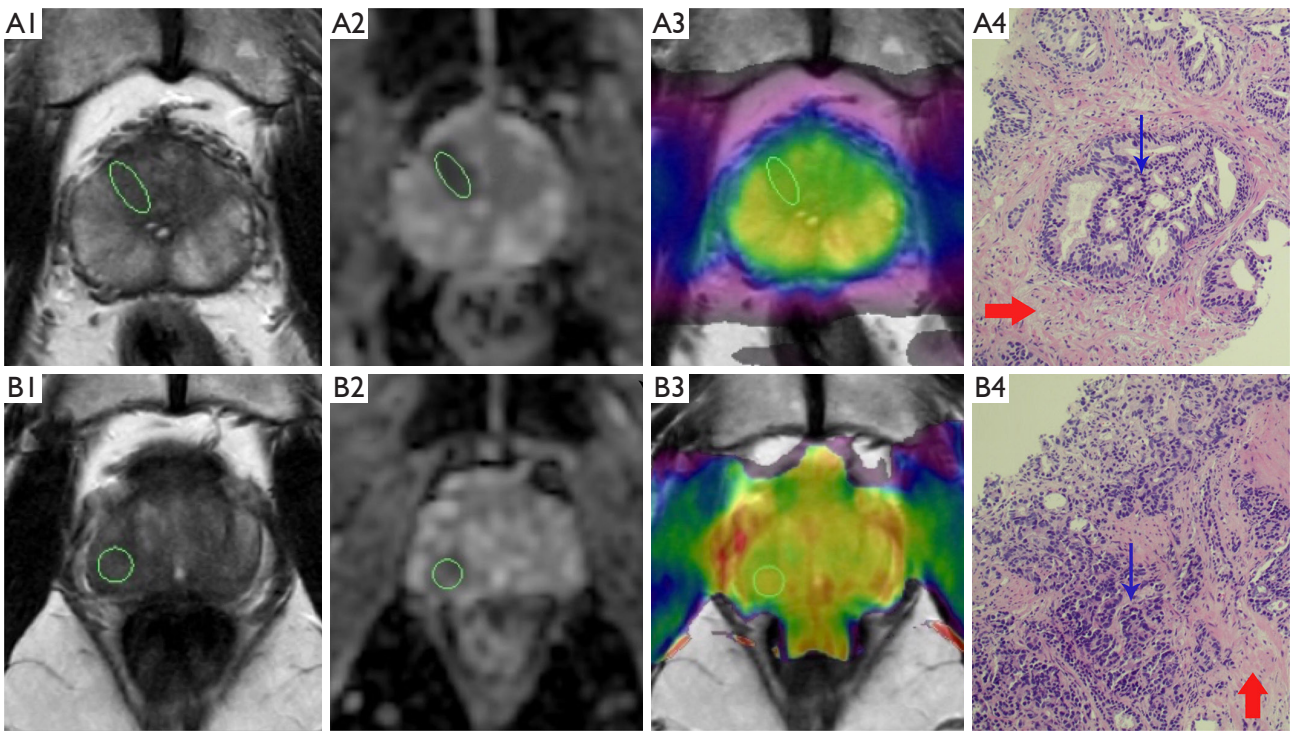

Figure 3 Indications of the definition of the regions of interest for parameter analyses. (A) Transitional zone prostate cancer with GG =2: (A1) the lesion appeared hypointense on the T2-weighted image; (A2) ADC image (ADC =0.87×10^{-3} mm^2/s); (A3) APT-weighted image with a T2WI overlay (APT =3.18%); (A4) corresponding pathological pictures (HE staining; magnification =200; the thick arrow shows the normal prostatic stroma, and the fine arrow shows the cribriform arrangement of tumor cells). (B) Peripheral zone prostate cancer with GG =5: (B1) the lesion appeared isointense on the T2W; (B2) ADC image (ADC =1.12×10^{-3} mm^2/s); (B3) APT-weighted image with a T2WI overlay (APT =4.27%); (B4) corresponding pathological pictures (HE staining; magnification =200; the thick arrow shows the normal prostatic stroma and the fine arrow shows the trabecular-like arrangement of tumor cells). ADC, apparent diffusion coefficient; APT, amide proton transfer; GG, grade group; HE, hematoxylin and eosin; T2WI, T2-weighted imaging.

PCa lesions by their signal intensity in T2, DWI, and ADC images and then confirmed whether these nodules were located within tissues that the surgical or biopsy obtained for the pathological diagnosis.

The APT parameter magnetization transfer ratio with asymmetric analysis (MTRasym 3.5 ppm) was calculated using the following equation (15).

$$\mathrm{MTRasym}(3.5\ \mathrm{ppm})=\left[S_{at}(-3.5\ \mathrm{ppm})-S_{at}(+3.5\ \mathrm{ppm})\right]/S_0 \quad [1]$$

where S_0 is the signal intensity without the saturation pulse, S_{sat} is the signal intensity after applying the saturation pulse, and MTRasym (3.5 ppm) is the magnetization transfer ratio asymmetry at 3.5 ppm.

Histopathology evaluation

All surgical specimens were examined by 1 pathologist (Lei Zhao, with 18 years of experience) who was blinded to the clinical and imaging data. All the specimens were fixed in formalin, cut into 4 to 5-μm sections, and stained with hematoxylin and eosin (HE). The pathologist outlined the zonal origin and GG for all tumor foci. The GG of each tumor foci was recorded as GG =1, GG =2, GG =3, or GG ≥4. Finally, all tumor foci were divided into a GG ≤2 or a GG ≥3 for analysis (16,17) due to the prognostic differences between these 2 groups.

Statistical analysis

All data were analyzed using SPSS 21.0.0 (IBM Corp., Armonk, NY, USA), and graphics were drawn using GraphPad Prism version 9.0.2 (GraphPad Software Inc., San Diego, CA, USA). We conducted an a priori power analysis to test the adequacy of our sample size to an independent sample *t*-test using G*Power 3.1 software (18). We specified an alpha level of 0.05, a 1–β error probability of 0.80, and an effect size (*f*) of 0.50 for an estimated medium effect. The results of the analysis suggested a total recommended sample size of 128. A post hoc power analysis revealed that a sample size of 180 (GG ≤2, n=71; GG ≥3; n =109) would result in a reported power of 0.893 to detect a medium effect (*f*=0.50) with α at 0.05.

The APT, ADC, T2*, total PSA, PSA density, and age of patients are expressed as the mean and standard deviation. The normal distribution of the data was tested using the Kolmogorov-Smirnov method. After testing for normality, the independent samples *t*-test was applied to analyze the statistical differences in the demographic and MRI parameters.

We selected the independent predictors and established the diagnostic efficacy as follows. First, a univariate analysis regression model was established to analyze the correlation between the MRI parameters of the GG ≤2 and GG ≥3. Second, multivariate logistic regression analyses were applied to identify independent predictors of the MRI parameters and combined parameters of the GG ≤2 and the GG ≥3. Factors with P<0.05 on the univariate analysis were used as the input variables for the multiple logistic regression analysis. After the final model was selected with the forward selection, model I [APT-weighted (APTw)], model II (1/ADC), and model III (APTw + 1/ADC) were established. Finally, binary logistic regression was used to calculate the prediction probability of the above model, the receiver operator characteristic (ROC) curve was drawn by predicting the probability, and the joint diagnostic efficacy was analyzed. The Youden index was calculated according to the following equation: Youden index = sensitivity + specificity –1. The optimal cutoff value was selected based on the maximum value of the Youden index. Differences in the area under the ROC curve (AUC) of the MRI parameters were analyzed using the Delong test. A P value <0.05 was considered statistically significant.

Results

Demographic characteristics

The study enrolled 180 patients with PCa who were divided into 2 groups stratified by GG, with 71 cases in GG ≤2 and 109 cases in GG ≥3. After stratification by the zonal origin of the PCa, there were 57 cases of TZ origin, which included 21 cases in GG ≤2 and 36 cases in GG ≥3. There were 123 cases of PZ origin, which included 50 cases in GG ≤2 group and 73 cases in GG ≥3 group. The demographic characteristics of patients are shown in *Table 2*.

Comparative analysis of characteristic and radiologic parameters

A comparison of the characteristics and radiologic parameters of TZ PCa is shown in *Table 3*. The APT values in GG ≤2 were significantly lower than those in GG ≥3 (2.97±0.57 *vs.* 3.78±0.95; P=0.001), while the ADC values in GG ≤2 were significantly higher than those in GG ≥3 (0.89±0.19 *vs.* 0.71±0.12; P<0.001). A comparison of the characteristics and radiologic parameters of PZ

Table 2 Demographic characteristics and radiologic parameters

Characteristics	GG ≤2 (n=71)	GG ≥3 (n=109)	χ^2/t value	P value
Demographic, mean ± SD				
Age (years)	67.03±8.696	69.60±9.638	1.81	0.07
Clinical, mean ± SD				
PSA density (ng/mL^3)	0.17±0.14	0.16±0.12	0.19	0.89
Radiologic, mean ± SD				
APTw (%)	3.05±0.45	3.72±0.61	7.88	<0.001*
ADC (×10^{-3} mm^2/s)	1.01±0.20	0.81±0.21	6.21	<0.001*
T2* (ms)	52.38±9.62	49.59±9.87	1.87	0.06
Zone of origin, n (%)				–
PZ PCa	50 (70.42)	73 (66.97)		
TZ PCa	21 (29.58)	36 (33.03)		
Grade group, n (%)				–
GG =1	43 (60.56)	–		
GG =2	28 (39.44)	–		
GG =3	–	37 (33.94)		
GG ≥4	–	72 (66.06)		

, comparison with statistical significance. PSA density was calculated as total PSA divided by prostate volume. GG, grade group; PSA, prostate-specific antigen; APTw, amide proton transfer-weighted; ADC, apparent diffusion coefficient; T2, quantitative T2*; TZ PCa, transitional zone prostate cancer; PZ PCa, peripheral zone prostate cancer; SD, standard deviation.

Table 3 Characteristics and radiologic parameters of Tz PCa

Characteristic	GG ≤2 (n=21)	GG ≥3 (n=36)	χ^2/t value	P value
Age (years), mean ± SD	66.3±7.59	70.64±8.20	1.96	0.54
t-PSA (ng/mL), mean ± SD	9.47±5.90	11.95±8.09	1.22	0.22
PSA density (ng/mL^3), mean ± SD	0.18±0.10	0.20±0.14	0.75	0.45
APTw mean (%), mean ± SD	2.97±0.57	3.78±0.95	3.45	0.001*
ADC (×10^{-3} mm^2/s), mean ± SD	0.89±0.19	0.71±0.12	4.24	<0.001*
T2* (ms), mean ± SD	53.67±7.73	49.54±7.80	1.93	0.06

, comparison with statistical significance. PSA density was calculated as total PSA divided by prostate volume. GG, grade group; t-PSA, total prostate-specific antigen; APTw, amide proton transfer-weighted; ADC, apparent diffusion coefficient; T2, quantitative T2*; TZ PCa, transitional zone prostate cancer; SD, standard deviation.

PCa are shown in *Table 4*. The APT values in GG ≤2 were significantly lower than those in GG ≥3 (3.09±0.40 *vs.* 3.71±0.36; P<0.001), and the ADC values in GG ≤2 were significantly higher than those in the GG ≥3 (1.06±0.18 versus 0.86±0.22; P<0.001).

Correlation analysis of parameters stratified by International Society of Urological Pathology GG

In TZ PCa, APT [odds ratio (OR) =3.20; 95% confidence interval (CI): 1.14–8.98; P=0.02] and ADC values (OR =89.79, 95% CI: 2.85–2,827.99; P=0.01) were independent

Table 4 Characteristics and radiologic parameters of Pz PCa

Characteristics	GG ≤2 (n=50)	GG ≥3 (n=73)	χ^2/t value	P value
Age (years), mean ± SD	67.32±9.188	69.08±10.28	0.974	0.32
t-PSA (ng/mL), mean ± SD	9.09±8.93	9.40±8.76	0.19	0.85
PSA density (ng/mL^3), mean ± SD	0.14±0.13	0.15±0.12	0.32	0.44
APTw mean (%), mean ± SD	3.09±0.40	3.71±0.36	8.91	<0.001*
ADC ($\times10^{-3}$ mm^2/s), mean ± SD	1.06±0.18	0.86±0.22	3.23	<0.001*
T2* (ms), mean ± SD	52.55±9.97	51.70±9.56	0.47	0.64

, comparison with statistical significance. PSA density was calculated as total PSA divided by prostate volume. GG, grade group; t-PSA, total prostate-specific antigen; APTw, amide proton transfer-weighted; ADC, apparent diffusion coefficient; T2, quantitative T2*; PZ PCa, peripheral zone prostate cancer; SD, standard deviation.

Table 5 Logistic analysis of parameters stratified by grade group

Parameters	TZ PCa		PZ PCa	
	OR (95% CI)	P value	OR (95% CI)	P value
APTw	3.20 (1.14–8.98)	0.02*	86.32 (13.24–562.88)	0.003*
1/ADC	89.79 (2.85–2,827.99)	0.01*	39.92 (3.22–494.18)	0.004*

*, comparison with statistical significance. APTw, amide proton transfer-weighted; ADC, apparent diffusion coefficient; TZ PCa, transitional zone prostate cancer; PZ PCa, peripheral zone prostate cancer; OR, odds ratio; CI, confidence interval.

predictors of discriminating GG ≤2 from GG ≥3 (*Table 5*). In PZ PCa, APT (OR =86.32, 95% CI: 13.24–562.88; P=0.003) and ADC values (OR =39.92; 95% CI: 3.22–494.18, P=0.004) were independent predictors of discriminating GG ≤2 from GG ≥3 group (*Table 5*).

ROC analysis

ROC analyses assessing the diagnostic efficacy of APT and ADC to discriminate GG ≤2 from GG ≥3 in TZ PCa and PZ PCa are summarized in *Table 6*.

In TZ PCa, the AUC of APT and ADC (0.743 and 0.774, respectively) showed no significant differences in the Delong test. However, the diagnostic sensitivity and specificity of APT and ADC were different. At the optimal cutoff values of 3.35% and 1.25×10^{-3} mm^2/s, the sensitivity and specificity of APT were 61.1% and 81.0%, respectively, and those of ADC were 83.3% and 61.9%, respectively, the AUC of the combination of APT and ADC was 0.866, which was significantly higher than the AUC of APT and ADC as shown by the Delong test. The P values of the combined model with APT and ADC were 0.002 and 0.020, respectively (*Figure 4*; *Table 7*).

In PZ PCa, the AUC of APT and ADC were 0.878 and 0.760, respectively. There were significant differences between APT and ADC in the Delong test. At the optimal cutoff values of 3.31×10^{-3} and 0.79×10^{-3} mm^2/s, the sensitivity and specificity of APT were 74.0% and 83.6%, respectively, and those of ADC were 94.0% and 53.4%, respectively. Differences in AUC in the Delong test were found between APT, ADC, and the combination of APT and ADC. The P value of Delong test between APT with ADC values was 0.014. The P values of the combined model with APT and ADC values in Delong test were P=0.033 and P<0.001, respectively (*Figure 5*; *Table 7*).

Discussion

We evaluated the difference and association between APT and ADC in discriminating PCa grades. The APT values in GG ≤2 were significantly lower than those in GG ≥3, while the ADC values in GG ≤2 were significantly higher than those in GG ≥3. APT and ADC were independent predictors of PCa differentiation. A combination model of APT and ADC improved the diagnostic efficacy of PCa differentiation in TZ and PZ PCa. In addition, APT and ADC had a complementary effect in the sensitivity and specificity of identifying different risk groups of PCa.

Table 6 ROC analysis of the diagnostic performance for different parameters and model for distinguishing GG ≤2 from GG ≥3

Parameters	AUC	Cutoff ($\times10^{-3}$ mm^2/s)	Sensitivity (%)	Specificity (%)	True positive (%)	False positive (%)	True negative (%)	False negative (%)	95% CI	P value
TZ PCa										
APTw	0.743	3.35	61.1	81.0	61.1	38.9	80.9	19.0	0.615, 0.870	0.002*
1/ADC	0.774	1.25	83.3	61.9	66.7	33.3	61.9	38.1	0.646, 0.903	0.001*
Combined model	0.866	–	88.9	76.2	22.2	77.8	95.2	4.8	0.791, 0.971	<0.001*
PZ PCa										
APTw	0.878	3.31	74.0	83.6	82.2	17.8	74.0	26.0	0.819, 0.918	<0.001*
1/ADC	0.760	0.79	94.0	53.4	95.9	4.1	14.0	86.0	0.678, 0.843	<0.001*
Combined model	0.901	–	79.5	88.0	79.5	20.5	90.0	10.0	0.849, 0.954	<0.001*

*, comparison with statistical significance. ROC, receiver operating characteristic; AUC, area under the curve; APTw, amide proton transfer-weighted; ADC, apparent diffusion coefficient; TZ PCa, transition zone prostate cancer; PZ PCa, peripheral zone prostate cancer; GG, grade group.

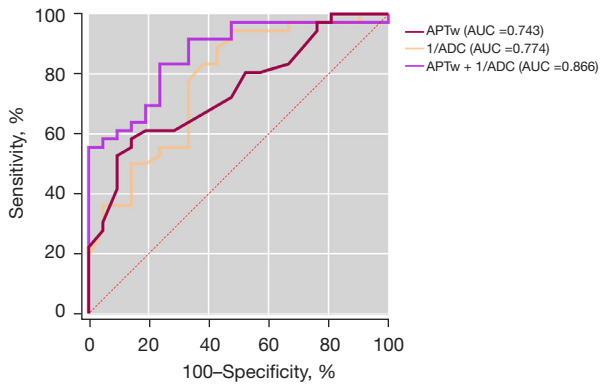

Figure 4 ROC analyses for assessing the diagnostic efficacy of MR parameters in the transitional zone prostate cancer GG. ADC, apparent diffusion coefficient; APTw, amide proton transfer-weighted; AUC, area under the curve; GG, grade group; MR, magnetic resonance; ROC, receiver operating characteristic.

Table 7 Delong test of the diagnostic efficacy between parameters and the combined model

Parameters	Z statistic	P value
TZ PCa		
APTw *vs.* combined model	3.030	0.002*
1/ADC *vs.* combined model	2.315	0.020*
APTw *vs.* 1/ADC	0.381	0.703
PZ PCa		
APTw *vs.* combined model	2.126	0.033*
1/ADC *vs.* combined model	4.441	<0.001*
APTw *vs.* 1/ADC	2.459	0.014*

*, comparison with statistical significance. APTw, amide proton transfer-weighted; ADC, apparent diffusion coefficient; TZ PCa, transition zone prostate cancer; PZ PCa, peripheral zone prostate cancer.

ADC correlates with the tumor grade and is predominantly affected by cellular-level water diffusion. APT imaging reflects the increased protein and peptide concentrations produced by the abnormal tumor cell proteosynthesis due to mitotic activity and cell metabolism, which is altered in high-grade tumors (13). On the one hand, APT is not as sensitive as ADC in reflecting cellular density and molecular diffusion. On the other hand, APT imaging was shown to provide unique information about the presence of PCa, which is complementary to ADC and showed more diagnostic efficacy in differentiating the grades of PCa. Theoretically, APT imaging may be more specific for detecting not only cellular density, but also tumor cell proliferation rates that lead to overall elevated mobile protein levels. Finally, in the present study, APT showed higher diagnostic performance (compared to ADC for distinguishing the 2 PCa groups in PZ PCa (AUC: 0.878 *vs.* 0.760). Wu *et al.* (32) reported that APT showed the highest AUC (AUC: 0.890; 95% CI: 0.805–0.947) in differentiating low- from high-grade hepatocarcinoma, which is consistent with our results of PCa differentiation. Boesen *et al.* (8)

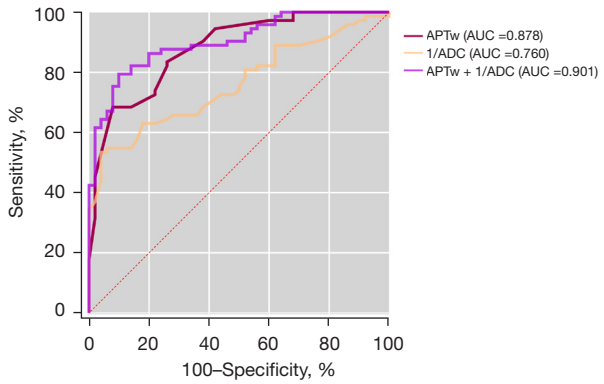

Figure 5 ROC analyses for assessing the diagnostic efficacy of MR parameters in the peripheral zone prostate cancer GG. ADC, apparent diffusion coefficient; APTw, amide proton transfer-weighted; AUC, area under the curve; GG, grade group; MR, magnetic resonance; ROC, receiver operating characteristic.

Previous studies demonstrated that APT values could provide more accurate lesion characterization in discriminating TZ PCa from benign prostatic hyperplasia (19). Theoretically, as malignant tumors become more poorly differentiated and the proliferation rate, cellular density, and nuclear-to-cytoplasmic ratios increase, the upward trend in APT values may be more significant (20). As expected, in the present study, the APT values in GG ≤2 were significantly lower than those in GG ≥3 group both in TZ and PZ PCa. Takayama *et al.* (14) reported that, as PCa differentiation decreased, the APT values first increased and then decreased, and the mean APT values in PCa with a Gleason score of 7 were higher than those for the other Gleason score groups. The APT values in Takayama *et al.*'s study did not show a significant rank correlation with the Gleason score groups, which differed from those studies involving APT imaging of other malignant tumors (19,21-23). This trend was not found in our study because there were only 2 GGs, but our results still showed significant differences between GG ≤2 and GG ≥3. Another study based on Chinese patients reported that APT values of the low-, medium-, and high-risk groups increased gradually (24). Consistent with our results, these initial findings indicate that APT imaging for PCa has the unique potential to become a valuable imaging marker for categorizing different risk PCa groups.

Numerous studies have validated that ADC is a valuable quantitative parameter that can be used to assess the degree of differentiation in PCa and other malignant tumors (8,23,25). Similar to reports in existing literature, our study showed that the ADC values in GG ≤2 were significantly higher than those in GG ≥3. Moreover, the binary logistic analyses showed both APT and ADC values were independent predictors of PCa differentiation, but there were several differences between APT and ADC values in discriminating PCa GG groups. First, APT and ADC values had different ORs with GGs in PCa originating in different zones. The OR of APT and ADC correlated to PCa grades in the TZ and PZ PCa were 3.20 *vs.* 89.79 and 86.32 *vs.* 39.92, respectively.

Theoretically, APT is influenced by mobile protein levels, temperature, and pH values (26). However, the intracellular pH is almost the same as that in the different tumors or different tumor grades. Therefore, the contribution of the possible pH variation to the measured APT imaging contrast may be minimal (11). Another factor affecting APT MRI signals is the T1 relaxation time, which may be reduced in regions of calcification and microbleeding that more frequently occur in TZ than PZ (11,26). Shortening the T1 relaxation time can reduce APT values and the detectability of mobile protein levels (11). In addition, the different OR associations between ADC and GG in peripheral and transitional PCa may indicate that possible different tumor behavior is displayed by DWI between the different localizations of PCa (27,28). Another reason for the different OR association may be that spatial density and the diversity of architectural histology in different PCa zones could influence DWI (29). Furthermore, APT and ADC yielded discrepant sensitivity and specificity values in the ROC analysis for TZ and PZ PCa differentiation in our study.

Our results showed that APT had lower sensitivity and higher specificity than did ADC. In contrast, ADC had higher sensitivity and lower specificity in identifying different GG groups in TZ and PZ PCa. Yin *et al.* (24) reported that the sensitivity and specificity of APT in differentiating a low-middle PCa risk group were 80.00% and 92.86%, respectively. In the middle-high PCa risk group, the sensitivity and specificity were 64.29% and 92.00%, respectively. These results are consistent with those of our study. Similar conclusions about the sensitivity and specificity of ADC in differentiating the risk groups of patients with PCa have been reported in several studies (30,31).

The differences in sensitivity and specificity may occur because these 2 parameters reflect different pathophysiological statuses. ADC and APT reportedly reflect different aspects of the tumor microenvironment (13).

reported that the AUC was 0.72 (95% CI: 0.62–0.82) for the ADC value in discriminating PCa between GG ≤2 and GG ≥3, which was similar to our results of about 0.774 in TZ PCa and 0.760 in PZ PCa. In addition, the cutoff value of APT for the best diagnostic efficacy was 3.35 in TZ PCa and 3.31 in PZ PCa, which showed more repeatability than did the ADC cutoff value of 1.55 in TZ PCa and 0.79 in PZ PCa. Yin *et al.* (24) reported that the cutoff values of APT when differentiating low to middle-risk PCa from middle to high-risk PCa were 3.35 and 3.45, respectively, which were similar to our results. Overall, APT appears to have superior diagnostic efficacy and repeatability to ADC in assessing PCa differentiation.

APT showed good specificity in PCa risk stratification and better reproducibility of the cutoff value in TZ and PZ PCa than did ADC values; however, the AUC of APT still varied when differentiating PCa of different zonal origins. It seems that the diagnostic efficacy of APT in the PZ was greater than that in the TZ. The AUC in the PZ was 0.878, while that in the in TZ was 0.743. The variability in ADC values depended on the prostatic zone, which is consistent with other reported results (9). However, studies focusing on the differences and mechanisms of the diagnostic efficacy of APT in PCa with different zonal origins are still lacking. This lack of studies may be related to the different tumor behavior of PCa of different zonal origins (27,28). In addition, different tissue backgrounds in different prostate zones, such as more glands in PZ and more interstitial fibers in TZ, may also affect the diagnostic efficacy of APT.

In this study, the combination model of APT and ADC values yielded the highest diagnostic performance for distinguishing GG ≤2 from GG ≥3, with an AUC of 0.866 in TZ PCa and 0.901 in PZ PCa. Compared to those of ADC or APT values, the sensitivity and specificity of the combination model achieved a greater equilibrium between sensitivity and specificity. Predicting the GG based on ADC values is an area of research interest, but the reported data about the associations between ADC and GG are very inconsistent (25,31). By reflecting different pathophysiological statuses, the combined model of ADC and APT improved the diagnostic efficacy and balanced the sensitivity and specificity between the 2 parameters. Combined models are likely to have important clinical significance because higher sensitivity can reduce undertreatment, while higher specificity can guard against overtreatment.

Based on clinical settings, better risk stratification of PCa is a timely research topic for the reasonable management of patients with PCa. Multiparametric MRI is playing an increasingly important role in active surveillance to improve patient selection and enable effective monitoring. Previous studies indicate that diffusion and perfusion MR protocol has a certain but undefined role in PCa risk stratification (33,34). The overlap of perfusion patterns with benign lesions and tumor differentiation is the reason why the perfusion protocol is not a more common imaging sequence for PCa diagnosis, staging, and grading (35). Therefore, an APT-dependent imaging technique reflecting the specific molecular information of tumors could be a supplemental protocol for PCa risk stratification. Even though the potential clinical values of APT techniques are still limited. The real clinical values of amide chemical exchange saturation transfer (CEST) imaging that can be applied on all scanners of different vendors still require further study. Moreover, additional time consumption is another factor that needs to be weighed in clinical practice.

Strengths and limitations

The major strength of our study is that 4 REST slabs were used during APT scanning, which might partially improve the repeatability of APT values. The second strength is that the relationships between MRI parameters and PCa were examined based on the zonal origin of PCa. We also further investigated the diagnostic efficacy of the combined model after studying the differences and correlations of multiparameters between different GGs.

There are still several potential limitations. First, this was a single-center, single-scanner, single-vendor, and single-field strength analysis, and thus there is an increased chance of selection bias. Second, since a previous study suggested there was a bell-shaped correlation between APT and grade (13), only 2 GGs were used in the present study, which may cause confusion between other grade cutoff values. Third, the partial population in this study with predominantly high-grade disease does not reflect many populations of favorable risk-screened patients. Therefore, it is unclear whether these results can apply to all patients with PCa. Finally, the freehand ROI analysis used could have produced artificial errors, which could have affected the accuracy of the results.

Conclusions

APT and ADC have complementary effects on the sensitivity and specificity of identifying different PCa GGs.

APT values are better at identifying PZ PCa risk groups than are ADC values. A combination model of APT and ADC can improve the diagnostic efficacy in differentiating the grades of PZ PCa and TZ PCa.

Acknowledgments

The authors thank Lei Zhao (Pathology Department of Nanxishan Hospital of Guangxi Zhuang Autonomous Region) and Songbai Liao (Urology Department of Nanxishan Hospital of Guangxi Zhuang Autonomous Region) for their help and discussion.
Funding: None.

Footnote

Reporting Checklist: The authors have completed the STARD reporting checklist. Available at https://qims.amegroups.com/article/view/10.21037/qims-22-721/rc

Conflicts of Interest: All authors have completed the ICMJE uniform disclosure form (available at https://qims.amegroups.com/article/view/10.21037/qims-22-721/coif). The authors have no conflicts of interest to declare.

Ethical Statement: The authors are accountable for all aspects of the work in ensuring that questions related to the accuracy or integrity of any part of the work are appropriately investigated and resolved. The study was conducted in accordance with the Declaration of Helsinki (as revised in 2013). The study was approved by the Ethics Committee of Nanxishan Hospital of Guangxi Zhuang Autonomous Region, and informed consent was obtained from all participants.

References

1. Sciarra A, Cattarino S, Gentilucci A, Salciccia S, Alfarone A, Mariotti G, Innocenzi M, Gentile V. Update on screening in prostate cancer based on recent clinical trials. Rev Recent Clin Trials 2011;6:7-15.
2. Ploussard G, Epstein JI, Montironi R, Carroll PR, Wirth M, Grimm MO, Bjartell AS, Montorsi F, Freedland SJ, Erbersdobler A, van der Kwast TH. The contemporary concept of significant versus insignificant prostate cancer. Eur Urol 2011;60:291-303.
3. Cyll K, Löffeler S, Carlsen B, Skogstad K, Plathan ML, Landquist M, Haug ES. No significant difference in intermediate key outcomes in men with low- and intermediate-risk prostate cancer managed by active surveillance. Sci Rep 2022;12:6743.
4. Gacci M, Noale M, Artibani W, Bassi PF, Bertoni F, Bracarda S, et al. Quality of Life After Prostate Cancer Diagnosis: Data from the Pros-IT CNR. Eur Urol Focus 2017;3:321-4.
5. Cooperberg MR, Lin DW. Active Surveillance for Prostate Cancer: A 2020 Vision. Eur Urol 2020;77:687-8.
6. Porreca A, Colicchia M, Busetto GM, Ferro M. MRI and Active Surveillance for Prostate Cancer. Diagnostics (Basel) 2020.
7. Harmon SA, Brown GT, Sanford T, Mehralivand S, Shih JH, Xu S, Merino MJ, Choyke PL, Pinto PA, Wood BJ, McKenney JK, Turkbey B. Spatial density and diversity of architectural histology in prostate cancer: influence on diffusion weighted magnetic resonance imaging. Quant Imaging Med Surg 2020;10:326-39.
8. Boesen L, Chabanova E, Løgager V, Balslev I, Thomsen HS. Apparent diffusion coefficient ratio correlates significantly with prostate cancer gleason score at final pathology. J Magn Reson Imaging 2015;42:446-53.
9. Woo S, Kim SY, Cho JY, Kim SH. Preoperative Evaluation of Prostate Cancer Aggressiveness: Using ADC and ADC Ratio in Determining Gleason Score. AJR Am J Roentgenol 2016;207:114-20.
10. Ferro M, Lucarelli G, de Cobelli O, Vartolomei MD, Damiano R, Cantiello F, Crocerossa F, Perdonà S, Del Prete P, Cordima G, Musi G, Del Giudice F, Busetto GM, Chung BI, Porreca A, Ditonno P, Battaglia M, Terracciano D. Circulating preoperative testosterone level predicts unfavourable disease at radical prostatectomy in men with International Society of Urological Pathology Grade Group 1 prostate cancer diagnosed with systematic biopsies. World J Urol 2021;39:1861-7.
11. Jia G, Abaza R, Williams JD, Zynger DL, Zhou J, Shah ZK, Patel M, Sammet S, Wei L, Bahnson RR, Knopp MV. Amide proton transfer MR imaging of prostate cancer: a

preliminary study. J Magn Reson Imaging 2011;33:647-54.
12. Dou W, Lin CE, Ding H, Shen Y, Dou C, Qian L, Wen B, Wu B. Chemical exchange saturation transfer magnetic resonance imaging and its main and potential applications in pre-clinical and clinical studies. Quant Imaging Med Surg 2019;9:1747-66.
13. Choi YS, Ahn SS, Lee SK, Chang JH, Kang SG, Kim SH, Zhou J. Amide proton transfer imaging to discriminate between low- and high-grade gliomas: added value to apparent diffusion coefficient and relative cerebral blood volume. Eur Radiol 2017;27:3181-9.
14. Takayama Y, Nishie A, Sugimoto M, Togao O, Asayama Y, Ishigami K, Ushijima Y, Okamoto D, Fujita N, Yokomizo A, Keupp J, Honda H. Amide proton transfer (APT) magnetic resonance imaging of prostate cancer: comparison with Gleason scores. MAGMA 2016;29:671-9.
15. Zhou J, Payen JF, Wilson DA, Traystman RJ, van Zijl PC. Using the amide proton signals of intracellular proteins and peptides to detect pH effects in MRI. Nat Med 2003;9:1085-90.
16. Chan TY, Partin AW, Walsh PC, Epstein JI. Prognostic significance of Gleason score 3+4 versus Gleason score 4+3 tumor at radical prostatectomy. Urology 2000;56:823-7.
17. Rasiah KK, Stricker PD, Haynes AM, Delprado W, Turner JJ, Golovsky D, Brenner PC, Kooner R, O'Neill GF, Grygiel JJ, Sutherland RL, Henshall SM. Prognostic significance of Gleason pattern in patients with Gleason score 7 prostate carcinoma. Cancer 2003;98:2560-5.
18. Faul F, Erdfelder E, Lang AG, Buchner A. G*Power 3: a flexible statistical power analysis program for the social, behavioral, and biomedical sciences. Behav Res Methods 2007;39:175-91.
19. Guo Z, Qin X, Mu R, Lv J, Meng Z, Zheng W, Zhuang Z, Zhu X. Amide Proton Transfer Could Provide More Accurate Lesion Characterization in the Transition Zone of the Prostate. J Magn Reson Imaging 2022;56:1311-9.
20. Li B, Sun H, Zhang S, Wang X, Guo Q. Amide proton transfer imaging to evaluate the grading of squamous cell carcinoma of the cervix: A comparative study using (18) F FDG PET. J Magn Reson Imaging 2019;50:261-8.
21. Su C, Liu C, Zhao L, Jiang J, Zhang J, Li S, Zhu W, Wang J. Amide Proton Transfer Imaging Allows Detection of Glioma Grades and Tumor Proliferation: Comparison with Ki-67 Expression and Proton MR Spectroscopy Imaging. AJNR Am J Neuroradiol 2017;38:1702-9.
22. Nishie A, Takayama Y, Asayama Y, Ishigami K, Ushijima Y, Okamoto D, Fujita N, Tsurumaru D, Togao O, Manabe T, Oki E, Kubo Y, Hida T, Hirahashi-Fujiwara M, Keupp J, Honda H. Amide proton transfer imaging can predict tumor grade in rectal cancer. Magn Reson Imaging 2018;51:96-103.
23. Zhang H, Yong X, Ma X, Zhao J, Shen Z, Chen X, Tian F, Chen W, Wu D, Zhang Y. Differentiation of low- and high-grade pediatric gliomas with amide proton transfer imaging: added value beyond quantitative relaxation times. Eur Radiol 2021;31:9110-9.
24. Yin H, Wang D, Yan R, Jin X, Hu Y, Zhai Z, Duan J, Zhang J, Wang K, Han D. Comparison of Diffusion Kurtosis Imaging and Amide Proton Transfer Imaging in the Diagnosis and Risk Assessment of Prostate Cancer. Front Oncol 2021;11:640906.
25. Hambrock T, Somford DM, Huisman HJ, van Oort IM, Witjes JA, Hulsbergen-van de Kaa CA, Scheenen T, Barentsz JO. Relationship between apparent diffusion coefficients at 3.0-T MR imaging and Gleason grade in peripheral zone prostate cancer. Radiology 2011;259:453-61.
26. Goffeney N, Bulte JW, Duyn J, Bryant LH Jr, van Zijl PC. Sensitive NMR detection of cationic-polymer-based gene delivery systems using saturation transfer via proton exchange. J Am Chem Soc 2001;123:8628-9.
27. Sinnott JA, Rider JR, Carlsson J, Gerke T, Tyekucheva S, Penney KL, Sesso HD, Loda M, Fall K, Stampfer MJ, Mucci LA, Pawitan Y, Andersson SO, Andrén O. Molecular differences in transition zone and peripheral zone prostate tumors. Carcinogenesis 2015;36:632-8.
28. Lee JJ, Thomas IC, Nolley R, Ferrari M, Brooks JD, Leppert JT. Biologic differences between peripheral and transition zone prostate cancer. Prostate 2015;75:183-90.
29. Mayer R, Simone CB 2nd, Turkbey B, Choyke P. Correlation of prostate tumor eccentricity and Gleason scoring from prostatectomy and multi-parametric-magnetic resonance imaging. Quant Imaging Med Surg 2021;11:4235-44.
30. Karaarslan E, Altan Kus A, Alis D, Karaarslan UC, Saglican Y, Argun OB, Kural AR. Performance of apparent diffusion coefficient values and ratios for the prediction of prostate cancer aggressiveness across different MRI acquisition settings. Diagn Interv Radiol 2022;28:12-20.
31. Park H, Kim SH, Lee Y, Son JH. Comparison of diagnostic performance between diffusion kurtosis imaging parameters and mono-exponential ADC for determination of clinically significant cancer in patients with prostate cancer. Abdom Radiol (NY) 2020;45:4235-43.
32. Wu B, Jia F, Li X, Li L, Wang K, Han D. Comparative Study of Amide Proton Transfer Imaging and Intravoxel

Incoherent Motion Imaging for Predicting Histologic Grade of Hepatocellular Carcinoma. Front Oncol 2020;10:562049.
33. Wu LM, Xu JR, Ye YQ, Lu Q, Hu JN. The clinical value of diffusion-weighted imaging in combination with T2-weighted imaging in diagnosing prostate carcinoma: a systematic review and meta-analysis. AJR Am J Roentgenol 2012;199:103-10.
34. Bonekamp D, Jacobs MA, El-Khouli R, Stoianovici D, Macura KJ. Advancements in MR imaging of the prostate: from diagnosis to interventions. Radiographics 2011;31:677-703.
35. Haider MA, Yao X, Loblaw A, Finelli A. Multiparametric Magnetic Resonance Imaging in the Diagnosis of Prostate Cancer: A Systematic Review. Clin Oncol (R Coll Radiol) 2016;28:550-67.

Cite this article as: Qin X, Mu R, Zheng W, Li X, Liu F, Zhuang Z, Yang P, Zhu X. Comparison and combination of amide proton transfer magnetic resonance imaging and the apparent diffusion coefficient in differentiating the grades of prostate cancer. Quant Imaging Med Surg 2023;13(2):812-824. doi: 10.21037/qims-22-721

